

## Paired measurements of foraminiferal delta 18 O and Mg/Ca ratios of Indian monsoons reconstructed from Holocene to Last Glacial record

MAHESH Badanal<sup>1,\*</sup>, BANAKARVirupaxa<sup>1</sup>, BURR George<sup>2</sup>

<sup>1</sup> National Institute of Oceanography (CSIR), Dona Paula, Goa 403 004, India;

\* Corresponding author. E-mail: mahe687@gmail.com

<sup>2</sup> NSF-Arizona AMS Facility, 1118 East 4<sup>th</sup> Street, Tucson, AZ85721-0081, USA

**Abstract:** The effect of seasonally reversing monsoons in the northern Indian Ocean is to impart significant changes in surface salinity (SS). Here, we report SS changes during the last 32 kyr in the Lakshadweep Sea (southeastern Arabian Sea) estimated from paired measurements of  $\delta^{18}\text{O}$  and sea surface temperature (SST) utilizing *Globigerinoides sacculifer*, an upper mixed layer dwelling foraminifera. The heaviest  $\delta^{18}\text{O}_{G.sacculifer}$  ( $-0.07\pm 0.08\text{‰}$ ) is recorded between 23 – 15 ka BP, which could be defined as the last glacial maximum (LGM). The  $\delta^{18}\text{O}_{G.sacculifer}$  shift between the LGM and Holocene is 2.07 ‰. The SST shows an overall warming of 2 °C from the LGM to Holocene (28 °C to 30 °C). However, coldest SSTs are observed prior to LGM, i.e., ~27 ka BP. The SS was higher (~ 38 psu) throughout most of the recorded last glacial period (32.5 – 15 ka BP). This high salinity together with generally lower SSTs suggests a period of sustained weaker summer or stronger winter monsoons. The deglacial warming is associated with rapid reorganization of monsoons and is reflected in decreased salinity to a modern level of ~ 36.5 psu, within a period of ~ 5 kyr. This indicates intensification of summer monsoons during cold to warm climate transition.

**Key words:** Paleoclimate, Arabian Sea, Oxygen isotopes, Mg/Ca Thermometry, Monsoon variability.

## 1 Introduction

Semiannually reversing monsoon winds over the Arabian Sea (AS) modulate SST, SS and productivity in space and time (Wyrski, 1973). Modeling results have shown that an increase in monsoon wind intensity, whether summer or winter, induces surface cooling along with increased productivity in the AS (Murtugudde et al., 2007). The SS structure in the Eastern AS (EAS) is largely dictated by the presence of low-salinity tongue extending upto 15° N latitude (Fig. 1). The summer monsoons during interglacial periods were stronger than the glacial periods during which the winter monsoons were probably overwhelming (Banakar et al., 2005; Reichert et al., 1998; Emeis et al., 1995; Rostek et al., 1993; Anderson and Prell, 1993; Clemens and Prell, 1990; Prell and Van Campo, 1986; Duplessy, 1982). The robust proxy to monitor monsoon intensity could be the variation in SS as it instantly responds to changes in evaporation-precipitation. The SS can be reconstructed from the  $\delta^{18}\text{O}$  of seawater. The SST is an important component to be corrected while estimating  $\delta^{18}\text{O}$  of seawater from foraminiferal calcite. Reliable SSTs can be obtained using Mg/Ca ratios in planktonic foraminifera (Bijma et al., 1990; Bemis et al., 1998; Nurnberg et al., 1996; Elderfield and Ganssen, 2000). Only few SST estimates from the Mg/Ca method are available for the AS (Anand et al., 2008; Saher et al., 2007; Dahl and Oppo, 2006). In this paper we report the past-SST and -SS variations in the southeastern AS (Lakshadweep Sea) utilizing *G. sacculifer* picked from a sediment core and discuss their implication with respect to monsoon variability.

## 2 Materials and Method

An upper 150 cm section of a 552 cm long sediment core (SK129-CR05) retrieved on board ORV *Sagar Kanya* at 9° 21' N; 71° 59' E (Lakshadweep Sea: off Kochi, India) from a water depth of 2300 m (Fig. 1) is used for the present study. The sediment core was sub-sampled at 2 cm intervals except for the top peneliquid section, which was 4 cm thick. The calendar ages for the core are based on ten AMS- $^{14}\text{C}$  dates measured at the NSF-AMS facility, University of Arizona, USA. The radiocarbon dates were corrected for local reservoir age (600 yrs) (<http://intcal.qub.ac.uk>) and converted to calendar ages using the CalPal2007\_HULU calibration (Danzeglocke et al., 2007). The last dated section (149-151 cm) has yielded an age of  $32564 \pm 386$  cal y BP. The age of the core-top section (0-4 cm) is  $3048 \pm 67$  cal y BP (Fig. 2).

Around one hundred *G. sacculifer* tests (without terminal sac, size: 250-355  $\mu\text{m}$ ) from each section were handpicked under a binocular microscope. The tests were broke-open by gently pressing between two glass plates and homogenized with a fine brush. One third of the aliquot was used for oxygen isotope analysis and the remaining two third was subjected to cleaning required before Mg/Ca measurement. We have selected this particular species since the *G. sacculifer* is not only less susceptible to dissolution as compared to other planktonic species (Dekens et al., 2002; Delaney et al., 1985), but also the inter-chamber distribution of Mg/Ca is nearly uniform (Eggins et al., 2003). The SSTs were estimated using Dekens et al. (2002) *G.sacculifer*<sub>TROPICAL PACIFIC</sub> calibration ( $\text{Mg/Ca} = 0.37 \exp 0.09[\text{T} - 0.36(\text{core depth in km}) - 2 \text{ }^\circ\text{C}]$ ). This calibration is favored because the ocean-atmosphere coupled processes over the northern Indian Ocean are similar to that of the western tropical Pacific warm-pool (Webster and Fasullo, 2002). The Mg/Ca analyses were done at the ICP-OES laboratory of the National Institute of Oceanography (Goa), India. The oxygen isotope measurements were done at the Godwin Laboratory for Paleoclimate Research, University of Cambridge, UK. The measured  $^{18}\text{O}/^{16}\text{O}$  ratios are expressed as  $\delta^{18}\text{O}$  with reference to Vienna Pee Dee Belemnite (PDB). The precision of the  $\delta^{18}\text{O}$  measurements was  $\pm 0.08$  ‰. Previously published organic-carbon and -nitrogen data for the same sediment core (Pattan et al., 2003) were utilized to assess the monsoon-productivity relationship in the study region.

The cleaning steps for Mg/Ca analysis were performed following the method described by Barker et al. (2003). In brief, the stained and oxide-coated calcite fragments, visible clay lumps, and mineral grains were physically separated from the crushed aliquot and discarded. The clean fragments were washed five times with deionized water followed by methanol to remove clays. Organic coating was removed by treating the fragments with a buffered H<sub>2</sub>O<sub>2</sub>. The pre-dissolution Mg-polishing was done using 0.001 M HNO<sub>3</sub>. Before the dissolution in 1.5 ml of 0.75 M HNO<sub>3</sub>, the fragments were examined under the microscope to ensure that only the clean calcite was taken for dissolution. As the Mn-coated and stained fragments were removed initially, the oxide removal step was not incorporated. Finally the solution was centrifuged at ~ 10,000 rpm in order to eliminate even faint possibility of contamination by sub-micron (very fine) clay suspension.

All reagents used were of supra-pure quality. The solutions were analyzed on a Perkin-Elmer Optima 2000 DV ICP-OES calibrated with five multi-element calibration standards. The Mg/Ca ratios were obtained following the intensity-ratio calibration techniques described by DeVilliers et al. (2002). A quality control (QC) solution of Mg/Ca (= 5.144 mmol/mol) was analyzed after every 6 samples. The analytical error for Mg/Ca was within ± 0.6 %. The long-term average of QC (n = 67) measured during the analytical period yielded a mean of 5.111 ± 0.097 mmol/mol. The error on long term average of QC is 1.9 %. The Fe, Mn and Al were also measured to monitor the contamination. The scatter plots of Fe/Ca, Al/Ca and Mn/Ca (mmol/mmol) vs. Mg/Ca (mmol/mol) yielded insignificant correlations (R<sup>2</sup>= 0.011; 0.121 and 0.178) suggesting that the measured Mg/Ca ratios were free from contamination.

Local SS was estimated from the residual  $\delta^{18}\text{O}_{\text{seawater}}$ . The residual  $\delta^{18}\text{O}_{\text{seawater}}$  was calculated from the  $\delta^{18}\text{O}_{G.\text{sacculifer}}$  using Epstein et al. (1953) equation after subtracting the contribution from global ice volume (Shackleton, 2000) and measured SST. The residual  $\delta^{18}\text{O}_{\text{seawater}}$  was translated into salinity using Dahl and Oppo (2006) empirical equation. However, Rohling et al. (2000) have demonstrated that salinity estimation from seawater  $\delta^{18}\text{O}$  is less reliable than  $\delta^{18}\text{O}_{\text{seawater}}$  itself. Therefore, we place more emphasis on estimated  $\delta^{18}\text{O}_{\text{seawater}}$  than on the estimated salinity. The error on the salinity estimate is ±0.2 psu, hence we discuss only those SS variations which are above this limit.

### 3 Results and Discussions

Based on the depth variation of  $\delta^{18}\text{O}_{G.\text{sacculifer}}$ , the beginning of Holocene is recorded at 37 cm depth dating to 12 ka BP. The beginning of deglaciation occurs at a depth of 57 cm (~16 ka BP). The Marine Isotope Stage (MIS) 3/2 boundary is evident at 121 cm depth dating to 29 ka BP (Fig. 2). The LGM-Holocene  $\delta^{18}\text{O}_{G.\text{sacculifer}}$  difference is 2.07 ‰. This  $\delta^{18}\text{O}$  gradient incorporates 1.2 ‰ changes due to expanded global ice sheets during the glacial maximum and the remainder of 0.87 ‰ should therefore indicate changes in the local SS and SST. Conventionally, the recent-most heaviest  $\delta^{18}\text{O}_{G.\text{sacculifer}}$  event has been considered as the LGM. Instead, we have defined the LGM as a period recording the heaviest  $\delta^{18}\text{O}_{G.\text{sacculifer}}$  (-0.07‰) within the measurement precision band of ± 0.08 ‰ that covers a time-span of 23 – 15 ka BP. A similar observation has been made by Banakar et al. (2010) in another sediment core from the EAS. The  $\delta^{18}\text{O}_{G.\text{sacculifer}}$  transition from LGM to Holocene occurs as a rapid negative excursion beginning at 16 ka BP, leading into Holocene-minimum at 12 ka BP. The timings of LGM/Holocene and MIS-3/2 boundaries and the beginning of deglaciation are nearly consistent with the LR04 benthic  $\delta^{18}\text{O}$  stack (Lisiecki and Raymo, 2005).

The overall Mg/Ca varies between 3.1 and 4.5 mmol/mol, which translate into SST change of 27 °C to 30 °C. The SST obtained for core-top section (3.05 ka BP) is 30°C (Fig. 3) and is comparable to the modern SST at the core location, which falls in the equatorial warm-pool (Fig.1: <http://www.nodc.noaa.gov/WOA01>). The warmest average SST (~ 30 °C) is recorded during most of the Holocene and the colder SST (~ 28 °C) during the LGM and the coldest (~ 27 °C) during

the late MIS-3 and early MIS-2 (32 – 24 ka BP). The observed SST increase of 2 °C from LGM to Holocene is comparable with previously published SST gradients of 2-3 °C in the AS (Banakar et al., 2010; Saraswat et al., 2005; Rostek et al., 1993).

The time-series of SST exhibits step-increase from the coldest conditions (27 °C) to attain warmest Holocene conditions (~ 30 °C) at ~12 ka BP. The LGM SSTs show a fluctuation of 1°C around an average of ~28 °C (Fig. 3). Within the warm Holocene, an event of SST lowering of ~ 1 °C is recorded between 8.5 and 9.5 ka BP (Fig. 3) and is closely comparable with previous observation in the EAS (Banakar et al., 2010). This SST cooling within the Holocene appears to be a regional feature occurring across the AS, which has been interpreted as the surface cooling resulting from intensified monsoons (Dahl and Oppo, 2006; Overpeck et al., 1996).

There are three distinct warming events recorded within the LGM climate at ~ 21, ~ 18 and ~ 16 ka BP, which exhibit ~ 1 °C elevated SSTs above the average LGM SST of ~ 28 °C (Fig. 3). These warming events are similar to the warming events observed in western AS (WAS; Saher et al., 2007) though with some timing offsets. Intermittent weakening of winter winds, reduced upwelling in WAS, and inflow of warm water of South Equatorial origin have been invoked as the cause for these SST warming events (Saher et al., 2007). The winters during glacial periods are expected to be more intense and prolonged than during the interglacial times. The winter monsoon winds have profound influence on the SSTs of the AS under glacial conditions (Duplessy, 1982; Fontugne and Duplessy, 1986) and hence increased SSTs during the LGM period at the outset might suggest weakening of glacial winters. However, the C/N ratios (Fig. 4) do not clearly reflect any change expected during the period of weakened winter winds. Therefore, these warm-SST events within the LGM warrant detailed explanation that is presented in later part of the discussion.

Though the LGM SSTs were colder by ~ 1.5 °C as compared to Holocene average SST, the coldest SSTs (~27.5°C) are observed at 32 - 25 ka BP, i.e., prior to LGM. The lowest SSTs prior to LGM (late MIS 3 and early MIS 2) might have been the result of major cooling in response to most intense winter winds. A recent study of Clark et al. (2009) has show that the growth of global ice sheets to their maximum has occurred between ~33 and 26.5 ka and sustained at their maximum growth until ~20 ka. That is, the time period between 26.5 and 20 ka appears to be the actual global glacial maximum. The coldest SSTs observed during 32 to 25 ka BP in the present record may indicate influence of global climate cooling. However, such cooling appears unlikely in the present case because winter winds should have been most intense leading to increased basin-wide evaporation resulting in increased SS. On the contrary, the SS does not show any significant increase during 33-20 ka BP and remains nearly uniform around 37 psu until the beginning of deglaciation (Fig. 3). This observation suggests that the observed coldest SSTs were probably the result of intense upwelling in the EAS. This interpretation could be supported by an increased flux of biogenic-calcite and –opal during late MIS 3 recorded in the same sediment core (Pattan et al., 2003). The marginal fluctuations in SS prior to LGM may indicate intermittently varied upwelling primarily from the upper thermocline that consist mainly high salinity water originated in northern AS (Prasanna Kumar and Prasad, 1999). The role of low-salinity water inflow from the Bay of Bengal dictating observed SS fluctuations may be ruled out during this time as it was significantly reduced during the last glacial period (Chodankar et al., 2005).

The C/N ratios are ~ 8 throughout the Holocene and reach values up to 14 during the late MIS 3 (Pattan et al., 2003), which also records minimum SST. The Redfield ratio of C/N in marine organic matter is ~ 7 and >20 for terrestrial organic matter (Meyers, 1994). The diagenetic alteration of organic matter may also cause a variation in C/N ratios. However, the strong positive correlation between the C and N ( $r = 0.81$ ;  $n = 39$ , Fig. 5) rules out such alteration possibility. Hence, the higher C/N ratios during late MIS 3 must have been caused by increased abundance of terrestrial

organic matter in the sediment. From the X-Y plot of SST and SS against the C/N ratios (Fig. 6), it is observed that higher SSTs and lower SS correspond to lower C/N ratios and *vice-versa*. This in turn suggests that the relative strength of monsoon winds controls the variation of sedimentary C/N ratios in the EAS. The elevated C/N ratios during the glacial period are expected, as the glacial winter winds (land towards sea) might have been intense resulting in increased transfer of terrestrial organic matter in to the EAS (Banakar et al., 2005). An inverse relationship between SST and C/N ratios confirm that the most intense winter winds prevailed prior to LGM during which an upwelling event is also evident. The coherent association of C/N ratios with SSTs ( $r = 0.83$ ) further strengthen the interpretation that stronger winter winds prevailed during the late MIS 3. The lower C/N ratios associated with higher SSTs of the Holocene indicate the dominance of summer monsoons over winter monsoons leading to reduction in high C/N terrestrial organic matter in the sediment.

The SS estimated for the core-top section is 35.1 psu, which is similar to the modern SS at the core location (Fig. 1). The average Holocene SS is  $\sim 35.2$  psu, while it is 37.2 psu for the last glacial period. The SS time series shows marginal variation of  $\pm 0.2$  psu during the Holocene. The overall glacial-interglacial variability in SS is  $\sim 2$  psu, which is comparable with the previously observed SS gradient in the EAS (Banakar et al., 2010). The SS reaches the Holocene plateau at  $\sim 10$  ka BP, i.e., 3 ka later than the SST maximum. The decreasing trend of SS started at  $\sim 18$  ka BP, which is consistent with the beginning of deglaciation in LR04 Benthic record of Lisiecki and Raymo (2005). Also, the deglaciation and the Holocene plateau in SS trends follow the LR04 records.

Based on the observations made from the SS time-series (Fig. 3), it can be inferred that the E-P in the EAS has varied marginally during the Holocene. Within the LGM, the SS time-series shows distinct increase in salinity by about 0.2 to 0.6 psu occurring concurrently with the SST warming events of 21, 18 and 16 ka BP (Fig. 3). The coupled increases of SST and SS during the above events suggest distinctly different E-P balance than generally expected. In the modern or Holocene climate set-up the increased SSTs are associated with intensified summer monsoons, i.e., increased freshwater flux resulting in basin-wide decrease in the SS. We examine this set-up in light of previously suggested mechanism of warm-SST events within the cold LGM (Saher et al., 2007). The advection of south equatorial warm water into the EAS although can warm the SST, but cannot enhance the salinity because it is inherently less-saline water. If the warm-SST events were the result of intermittent weakening of the winter monsoons then also the salinity would decrease because of reduced evaporation. Interestingly, a recent study has identified regional sub-surface temperature inversion in the present study area (Lakshadweep Sea), where the sub-surface ( $\sim 40$  m) is warmer than the surface water (temperature inversion) and also saltier (see Nisha et al., 2009). Assuming an existence of this sub-surface temperature and salinity inversion during the LGM, the coupled increases in SST and SS in the Lakshadweep Sea may suggest vigorous mixing of sub-surface water with the surface layer. Durand et al. (2004) estimated that the heat trapped in the subsurface inversion in the Lakshadweep Sea could result in regional SST warming of over  $1^\circ\text{C}$  due to mixing. Therefore, the observed coupled increases in SST and SS at 21, 18 and 16 ka may indicate relatively intensified summer winds (intensified sub-surface mixing) within the LGM.

We examined the relationship of SST and SS with  $\delta^{18}\text{O}_{G.sacculifer}$  (Fig. 7). The SS association is found to be highly coherent and significant with  $\delta^{18}\text{O}_{G.sacculifer}$  ( $r = 0.94$ ;  $n=73$ ), while SST exhibits relatively less coherency ( $r = 0.60$ ;  $n = 73$ ). This observation suggests that the SST variability was mostly due to changes in local processes. The general trend of the SS time-series overlapping the  $\delta^{18}\text{O}_{G.sacculifer}$  time-series as well as the LR04 benthic oxygen isotope records indicate a close relationship between the evolution of SS and global ice-volume. However, the influences of local processes are also evident which are reflected as short-term distinct increases in SS during the glacial period as described above.

## 4 Conclusions

The SST time-series for Lakshadweep Sea (southeastern Arabian Sea) does not exhibit distinct glacial-interglacial variability suggesting dominance of local processes. The coupled increase in SST and SS within the LGM appears to be the result of mixing of warmer and saltier sub-surface water. Lowest SSTs prior to LGM likely indicate an intense upwelling. The SST cooling at ~ 9 ka BP within the warm Holocene is consistent with previous observation and indicates intensified monsoon winds. Our reconstructions indicate that the latest Holocene (3-4.7 ka BP) has witnessed rapid fluctuation in the summer monsoon intensity as evident in concomitant cooling of SST, lowering of SS, and decreasing  $\delta^{18}\text{O}_{G.sacculifer}$ .

## Acknowledgement

The samples used in this study were collected during the Cobalt-Crust cruises funded by the Ministry of Earth Sciences. The National Institute of Oceanography provided all logistic support. De-Martino Mitzi of Arizona University carried out AMS-radiocarbon measurements and Mike Hall of Cambridge University measured the oxygen isotopes. The useful comments by the anonymous reviewers are acknowledged. MB thanks EMR-CSIR for Junior/Senior Research Fellowship. This is NIO Contribution No: .....

## References

- Anand, P., Kroon, D., Singh, A.D., Ganeshram, R.S., Ganssen, G., and Elderfield, H., 2008. Coupled sea surface temperature–seawater  $\delta^{18}\text{O}$  reconstructions in the Arabian Sea at the millennial scale for the last 35 ka. *Paleoceanography*, 23: PA4207, doi: 10.1029/2007PA001564.
- Anderson, M.D., and Prell, L.W., 1993. A 300 ka record of upwelling off Oman during the Late Quaternary: Evidence of the Asian Southwest monsoon. *Paleoceanography*, 8: 193-208.
- Banakar, V.K., Mahesh, B.S., and Burr, G., 2010. Climatology of the Eastern Arabian Sea during the last glacial cycle reconstructed from paired measurement of foraminiferal  $\delta^{18}\text{O}$  and Mg/Ca. *Quaternary Research*, doi:10.1016/j.yqres.2010.02.002.
- Banakar, V.K., Oba, T., Chodankar, A.R., Kuramoto, K., Yamamoto, M., and Minagawa, M., 2005. Monsoon related changes in sea surface productivity and water column denitrification in the Eastern Arabian Sea during last glacial cycle. *Marine Geology*, 219: 99-108.
- Barker, S., Greaves, M., and Elderfield, H., 2003. A study of cleaning procedure used for foraminiferal Mg/Ca paleothermometry. *Geochemistry Geophysics Geosystems*, 4: doi: 10.1029/2003GC000559.
- Bijma, J., Faber, Jr W.W., and Hemleben, C., 1990. Temperature and salinity limits for growth and survival of some planktonic foraminifers in laboratory cultures. *Journal Foraminiferal Research*, 20: 95-116.
- Bemis, B.E., Spero, H.J., Bijma, J., and Lea, D.W., 1998. Re-evaluation of the oxygen isotopic composition of planktonic foraminifer: Experimental results and revised paleotemperature equations. *Paleoceanography*, 13: 150-160.
- Chodankar, A.R., Banakar, V.K., and Oba, T., 2005. Past 100 ka surface salinity gradient response in the Eastern Arabian Sea to the summer monsoon variation recorded by  $\delta^{18}\text{O}$  of *G. sacculifer*. *Global Planetary Change*, 47: 135-142.
- Clark, P. U., Dyke, A. S., Shakun, J. D., Carlson, A. E., Clark, J., Wohlfarth, B., Mitrovica, J., Hostetler, S. W., and McCabe, A. M., 2009. The Last Glacial Maximum. *Science*, 325: 710 DOI: 10.1126/science.1172873.
- Clemens, S.C., and Prell, W.L., 1990. Late Pleistocene Variability of Arabian Sea Summer Monsoon Winds and Continental Aridity: Eolian Records from the Lithogenic Component of Deep-Sea Sediments. *Paleoceanography*, 5: 109–145.

- Dahl, A.K., and Oppo, D.W., 2006. Sea surface temperature pattern reconstructions in the Arabian Sea. *Paleoceanography*, 21: PA1014, doi: 10.1029/2005PA001162.
- Danzeglocke, U., Jöris O and Weninger B 2008. CalPal-2007<sup>online</sup>. <http://www.calpal-online.de/>, 2008-10-05.
- DeVilliers, S., Greaves, M., and Elderfield, H., 2002. An intensity ration calibration method for the accurate determination of Mg/Ca and Sr/Ca of marine carbonates by ICP-AES. *Geochemistry Geophysics Geosystems*, 3: 2001GC000169.
- Dekens, P.S., Lea, D.W., Pak, D.K., and Spero, H.J., 2002. Core-top calibration of Mg/Ca in tropical foraminifera: Refining paleo-temperature estimation. *Geochemistry Geophysics Geosystems*, 3: 1022, doi: 10.1029/2001gC000200.
- Delaney, M.S., Be, A.W., and Boyle, E.A. 1985. Li, Sr, Mg and Na in foraminiferal calcite shells from laboratory culture, sediment traps and sediment cores. *Geochimica et Cosmochimica Acta*, 49: 1327-1341.
- Duplessy, J.C., 1982. Glacial to interglacial contrast in the northern Indian Ocean. *Nature*, 295: 464-498.
- Durand, F., Shetye, S. R., Vialard, J., Shankar, D., Shenoi, S. S. C. Ethe, C., and Madec, G., 2004. Impact of temperature inversions on SST evolution in the South-Eastern Arabian Sea during the pre-summer monsoon season. *Geophysical Research Letters*, 31: L01305, doi:10.1029/2003GL018906.
- Eggs, S., Deckker, P., and Marshall, J., 2003. Mg/Ca variation in planktonic foraminifera tests: Implications for reconstructing palaeo-seawater temperature and habitat migration. *Earth Planetary Science Letters*, 212: 291-306.
- Elderfield, H., and Ganssen, G., 2000. Past temperature and salinity using  $\delta^{18}\text{O}$  of surface ocean water inferred from foraminiferal Mg/Ca ratios. *Nature*, 405: 442-445.
- Emeis, K.C., Anderson, D.M., Doose, H., and Schulz, D., 1995. Sea-Surface Temperatures and the History of Monsoon Upwelling in the Northwest Arabian Sea during the Last 500,000 Years. *Quaternary Research*, 43: 355-361.
- Epstein, S., Buchsbaum, R., Lowenstam, A., and Urey, H.C., 1953. Revised carbonate-water isotopic temperature scale. *Bulletin of Geological Society of America*, 64: 1315-1325.
- Fontugne, M.R., and Duplessy, J.C., 1986. Variations of the monsoon regime during the upper Quaternary: Evidence from carbon isotopic record of organic matter in north Indian Ocean sediment cores. *Palaeogeography Palaeoclimatology Palaeoecology*, 56: 69-88.
- Lisiecki, L.E., and Raymo, M.E., 2005. A Pliocene-Pleistocene stack of 57 globally distributed benthic  $\delta^{18}\text{O}$  records. *Paleoceanography*, 20: PA1003: doi: 10.1029/2004PA001071.
- Meyers, P.A., 1994. Preservation of elemental and isotopic identification of sedimentary organic matter. *Chemical Geology*, 144: 213-302.
- Murtugudde, R., Seager, R., and Thoppil, P., 2007. Arabian Sea response to monsoon variations. *Paleoceanography*, 22: doi: 10.1029/2007PA001467.
- Nisha, K., Suryachandra A. R., Gopalakrishna, V. V., Rao, R. R., Girishkumar, M. S., Pankajakshan, T., Ravichandran, M., Rajesh, S., Girish, K., Johnson, Z., Anuradha, M., Gavaskar, S. S. M., Suneel, V., Krishna, S. M., 2009. Reduced Near-Surface Thermal Inversions in 2005-06 in the Southeastern Arabian Sea (Lakshadweep Sea). *Journal of Physical Oceanography*, 39: 1184-1199.
- Nürnberg, D., Bijma, J., and Hemleben, C., 1996. Assessing the reliability of magnesium in foraminiferal calcite as a proxy for water mass temperatures. *Geochimica et Cosmochimica Acta*, 60: 803-814.
- Overpeck, J.T., Anderson, D.M., Trumbore, S., and Prell, W.L., 1996. The southwest Indian monsoon over the last 18,000 years. *Climate Dynamics*, 12: 213-225.
- Pattan, J.N., Masuzawa, T., Naidu, P.D., Parthiban, G., and Yamamoto, M., 2003. Productivity fluctuations in the southeastern Arabian Sea during the last 140 ka. *Paleogeography Paleoclimatology Paleoecology*, 193: 575-590.
- Prasanna Kumar, S., and Prasad, T.G., 1999. Formation and spreading of Arabian Sea high salinity water mass. *Journal of Geophysical Research*, 104: 1455-1461.

- Prell, W.L., and Campo, E.V., 1986. Coherent response of Arabian Sea upwelling and pollen transport of late Quaternary monsoonal winds. *Nature*, 323: 526-528.
- Reichart, G.J., Lournes, L.J., and Zachariasse, W.J., 1998. Temporal variability in the northern Arabian Sea Oxygen Minimum Zone (OMZ) during the last 225,000 years. *Paleoceanography*, 13: 607–621.
- Rohling, E.J., 2000. Paleosalinity: confidence limits and future applications. *Marine Geology*, 163: 1-11.
- Rostek, F., Ruhland, G., Bassinot, F.C., Muller, P.J., Labeyrie, L.D., Lancelot, Y., and Bard, E., 1993. Reconstructing sea surface temperature and salinity using  $\delta^{18}\text{O}$  and alkenone records. *Nature*, 364: 319-321.
- Saraswat, R., Nigam, R., Weldeab, S., Mackensen, A., and Naidu, P.D., 2005. A first look at past sea surface temperatures in the equatorial Indian Ocean from Mg/Ca in foraminifera. *Geophysical Research Letters*, 32: doi: 10.1029/2005GL024039.
- Saher, M.H., Jung, S.J.A., Elderfield, H., Greaves, M., and Kroon, D., 2007. Sea surface temperatures of the western Arabian Sea during the last deglaciation. *Paleoceanography*, 22: PA2208, doi: 10.1029/2006PA001292.
- Shackleton, N.J., 2000. The 100,000 year ice-age cycle identified and found to lag temperature, carbon dioxide and orbital eccentricity. *Science*, 289: 1897-1902.
- Shankar, D., Vinayachandran, P.N., and Unnikrishnan, A.S., 2002. The monsoon currents in the north Indian Ocean. *Progressive Oceanography*, 52: 63-120.
- Webster, P.J., and Fasullo, J., 2002. Monsoons-Dynamic theory, in: Encyclopedia of atmospheric Sciences. *Academic Press*, 3: 1370-1385.
- Wyrtki, K., 1973. Physical oceanography of the Indian Ocean: The Biology of the Indian Ocean, B. Zeitzschel, (Ed.), Springer-Verlag, Berlin, 18-36.
- [www.nodc.noaa.gov/WOA01](http://www.nodc.noaa.gov/WOA01): Levitus and Boyer's Annual salinity and temperature online maps.

#### **About the First Author**

Mahesh Badanal                      Male: born in 1980: Doctoral Student at National Institute of Oceanography (HQ, Goa), a constituent laboratory of Council of Scientific and Industrial Research (New Delhi, India). The author is pursuing his PhD in Marine Sciences (Paleoclimate) with emphasis on reconstruction of past monsoons for the Late Quaternary.



## Captions to Figures

Fig. 1. SK129/CR05 sediment core location (star), shown on annual sea surface salinity (a) and surface temperature (b) maps of the Arabian Sea (AS) ([www.nodc.noaa.gov](http://www.nodc.noaa.gov)). Note the maximum SST region in which the present core lies. The northwestern AS shows the lowest SST (blue color code), while higher SSTs (red color code) are observed over the southwestern AS. Presence of low-salinity tongue along the west coast of India is evident by isohaline bordering the blue color region. The shaded block-arrows indicate modern reversing monsoon winds. Solid (broken) arrow indicates surface circulation during summer (winter) monsoons (Shankar *et al* 2002). The numbered filled circles are the locations of other sediment cores studied for Mg/Ca SST reconstructions [SK17 (Anand *et al* 2008); NIOP929 (Saher *et al* 2007)].

Fig. 2. The  $\delta^{18}\text{O}_{G.sacculifer}$  variation plotted against core depth (cm). The upward triangles along depth axis are the radiocarbon dated sections shown along with their calibrated calendar ages. The ages for remaining sections of the sediment core were obtained by calculating the sedimentation rates between two adjacent  $^{14}\text{C}$  dated sections. The broken vertical lines denote the marine oxygen isotope stage (MIS) boundaries.

Fig. 3. Composite plot of oxygen-isotope, SST (Red) and surface salinity (SS: blue) variations recorded in SK129/CR05 compared with LR04 benthic- $\delta^{18}\text{O}$  record (Lisiecki and Raymo, 2005). Vertical broken lines are the MIS 1/2 and 2/3 boundaries. LGM (shaded box) is the presently defined coldest event depicted by the heaviest  $\delta^{18}\text{O}_{G.sacculifer}$  variation. Only latest part of the MIS-3 is covered by the radiocarbon dated interval. The shaded boxes 1 to 3 in SST panel represent three warming events within the LGM. The numbered (4-6) blue color filled squares on LR04 benthic record indicate MIS boundaries: 4 = MIS1/MIS2, 5 = Beginning of deglaciation; 6 = MIS2/3.

Fig. 4. Time-series of SST (red), salinity (blue) and C/N ratios of sedimentary organic matter (black) in the studied sediment core. The C/N data is from Pattan *et al.* (2003). The shaded region indicates period of upwelling (high productivity) and intensified surface cooling (see text for details).

Fig. 5. Scatter plot of total organic carbon vs nitrogen.

Fig. 6. Scatter plots of C/N vs sea surface temperature (SST) and surface salinity (SS).

Fig. 7. Scatter plots of SST and SS vs  $\delta^{18}\text{O}_{G.sacculifer}$ .

AS-Arabian Sea; EAS-Eastern Arabian Sea; BoB-Bay of Bengal; SST-Sea Surface Temperature; SS-Surface Salinity; ASHSW-Arabian Sea High Saline Water; MIS-Marine Oxygen Isotope Stage; LGM-Last Glacial Maximum; C/N-Carbon/Nitrogen; E-P Evaporation minus Precipitation

Figures:

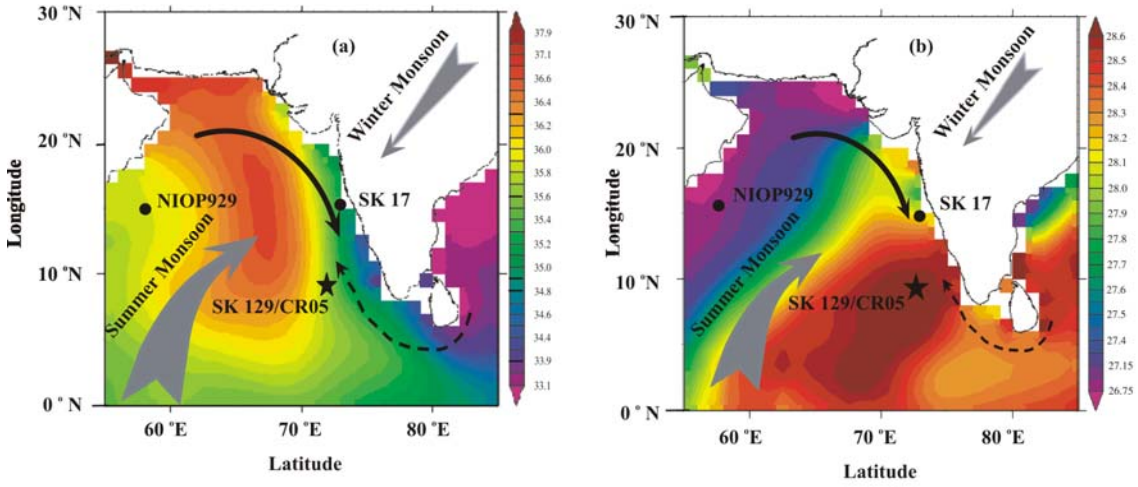


Fig.1.

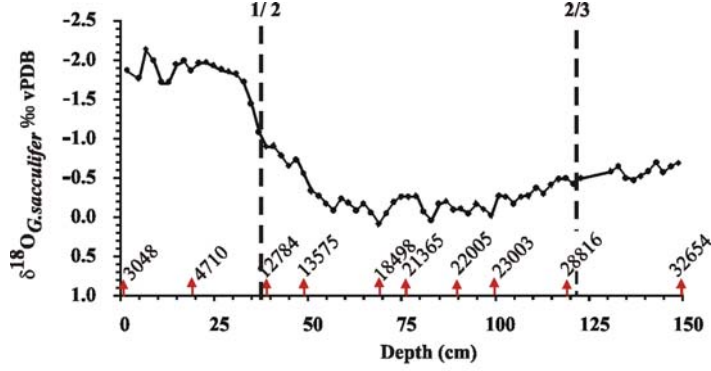


Fig.2

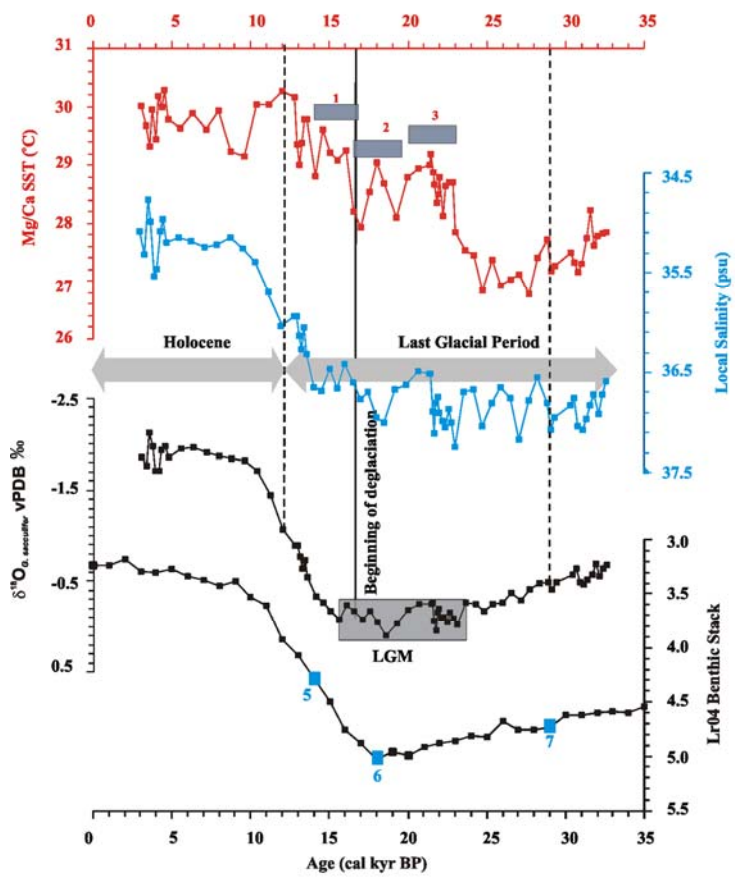


Fig.3.

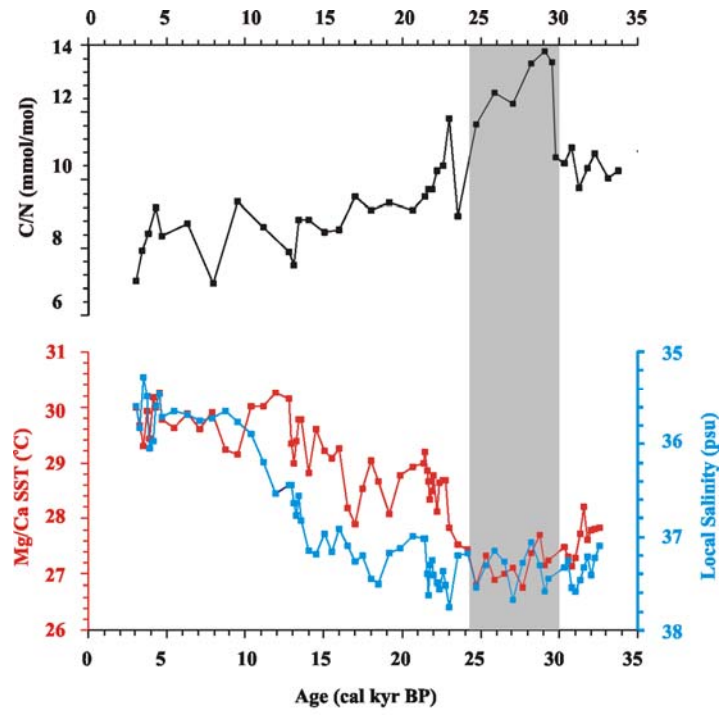


Fig.4.

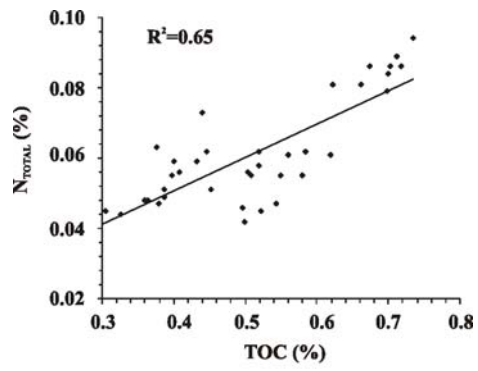


Fig.5.

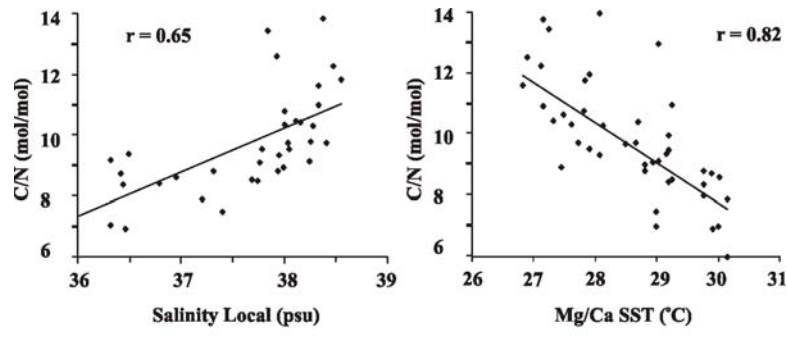


Fig.6.

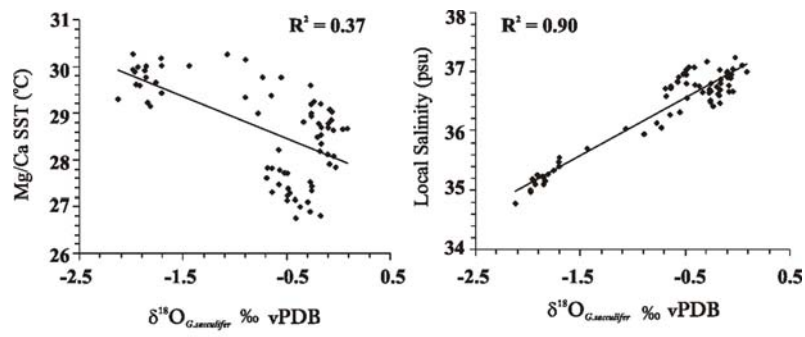


Fig.7.